RPW Science Performances

RPW-SYS-SOW-001518-LES
Iss. 2, Rev. 0

Prepared and approved after verification by all the Lead CoIs:	Function:	Signature:	Date
Milan Maksimovic	PI		15/05/2018
Verified by:	**Function:**	**Signature:**	**Date**
The RPW Lead CoIs			
Eric Lorfèvre Emmanuel Guilhem	System Engineer Science performances and EMC responsible		
For application:	**Function:**	**Signature:**	**Date**

CLASSIFICATION **PUBLIC** ☒ **RESTRICTED** ☐

l'Observatoire de Paris LESIA
Laboratoire d'Études Spatiales et d'Instrumentation en Astrophysique

CNRS-Observatoire de PARIS
Section de MEUDON – LESIA
5, place Jules Janssen
92195 Meudon Cedex – France

Change Record

Issue	Rev.	Date	Authors	Modifications
02		15/05/2018	M. Maksimovic	- Use of the data obtained with the RPW MEB Flight Model - Use of the effective antenna vectors as obtained by radio simulations - corredtion for a wrong value of the stray capacitance in the IDL program providing ΓL_{eff} - adding of the Antenna Thermo-mecahnical bending section - adding of the section on radio direction finding - adding of the section on RPW autocompatibility with respect to the Electro-magnetic Cleanliness

Acronym List

Acronym	Definition	Acronym	Definition
BIAS	Biasing Unit	MEB	Main Electronic Box
CNES	Centre National d'Etudes Spatiales	RPW	Radio & Plasma Waves instrument
EMC	Electro Magnetic Cleanliness	TDS	Time Domain Sampler
ESA	European Space Agency	TNR-HFR	Thermal Noise Receiver- High frequency receiver
LFR	Low Frequency Receiver		

Table of Contents

1 GENERAL

1.1 Scope of the Document

This document describes the RPW performances and compares them to the science requirements defined in [AD1].

Compared to the previous issue of this document, the current one is based on the measurements made on the final RPW MEB & SCM flight models and on updates simulations for both the DC/LF and radio domains of the electric antennas.

1.2 Applicable Documents

This document responds to the requirements of the documents listed in the following table:

Mark	Reference/Iss/Rev	Title of the document	Authors	Date
AD1	RPW-SYS-SRD-00040-LES Issue 02 rev 01	RPW Science Requirements	M. Maksimovic	12/06/2015
AD2				

1.3 Reference Documents

This document is based on the documents listed in the following table:

Mark	Reference/Iss/Rev	Title of the document	Authors	Date
RD1	SOLO-SY-TN-271-CNES Issue 03 Rev 00	Science Performance Justification	E. Guilhem & C. Fiachetti	12/02/2016
RD2	RPW-GEN-PPT-00075-LES Issue01, rev00	Effect of Antenna Tilt_on Direction Finding capabilities	V. Krupar et al.	19/10/2011
RD3	Proceedings of the 32nd URSI GASS, Montréal	On the Influence of the Antenna RPW/Solar Orbiter Tilt Angle and Thermal Bending to the Radio Direction Finding Capabilities	V. Krupar et al	19/08/2017
RD4	RADIO SCIENCE, VOL. 46, RS2008, doi:10.1029/2010RS004464, 2011	On the antenna calibration of space radio instruments using the galactic background: General formulas and application to STEREO/WAVES	A. Zaslavsky, N. Meyer-Vernet, S. Hoang, M. Maksimovic & S. D. Bale	18/03/2011
RD5	4000105622/12/NL/CBi	Anechoic chamber measurements of spaceborne antennas (CM/ANT), Final Report	M. Sampl	30/09/2013
RD6	SOLO-RPWSY-IF-55-CNES Issue 05, Rev. 03	Experiment Interface Document part B for RPW	B. Pontet	07/10/2015
RD7	RPW-SYS-MEB-DPS-NTT-000859-LES_Issue1_rev0_ DAS_User_Manual	DAS User Manual	C. Cuomo	
RD8	RPW-SYS-MEB-DPS-PRC-000529-LES_Ed3_Rev7	DAS Software Validation Specifications	J.-B. Viout	
RD9	RPW-SYS-MEB-DPS-PRC-000612-LES_Ed3_Rev2	DAS Software Validation Report	J.-B. Viout	
RD10		Antenna bending report by Stellar		

RD11	Scientific Report on FFG/ASAP 11 project SOLOCAL, Projektnummer: 847978	Calibration of the Solar Orbiter antennas by Rheometry and computer simulations (Scientific part)	M. Panchenko et al	04/2017
RD12			Plettemeir doc	
RD13	RPW-EAS-SYS-TN-001760-LES-MSSL Issue 02 Rev 01	Solar Orbiter / RPW and SWA EAS numerical simulations with the SPIS software	S. Guillemant	18/04/2017
RD14	RPW_ANT_Base_Capacitance_Proc_059 Ver. 1.4	Measurement of Antenna stray Capacitance	Stellar Scientific	
RD15				
RD16				
RD17				

2 MEB AND PRE-AMPLIFIERS PERFORMANCES

In this section we describe the measured Flight Model MEB + preamplifiers noise floors or sensitivities and dynamical ranges as provided by the LFR, TDS, TNR-HFR & SCM teams.

2.1 Sensitivities & noise floors

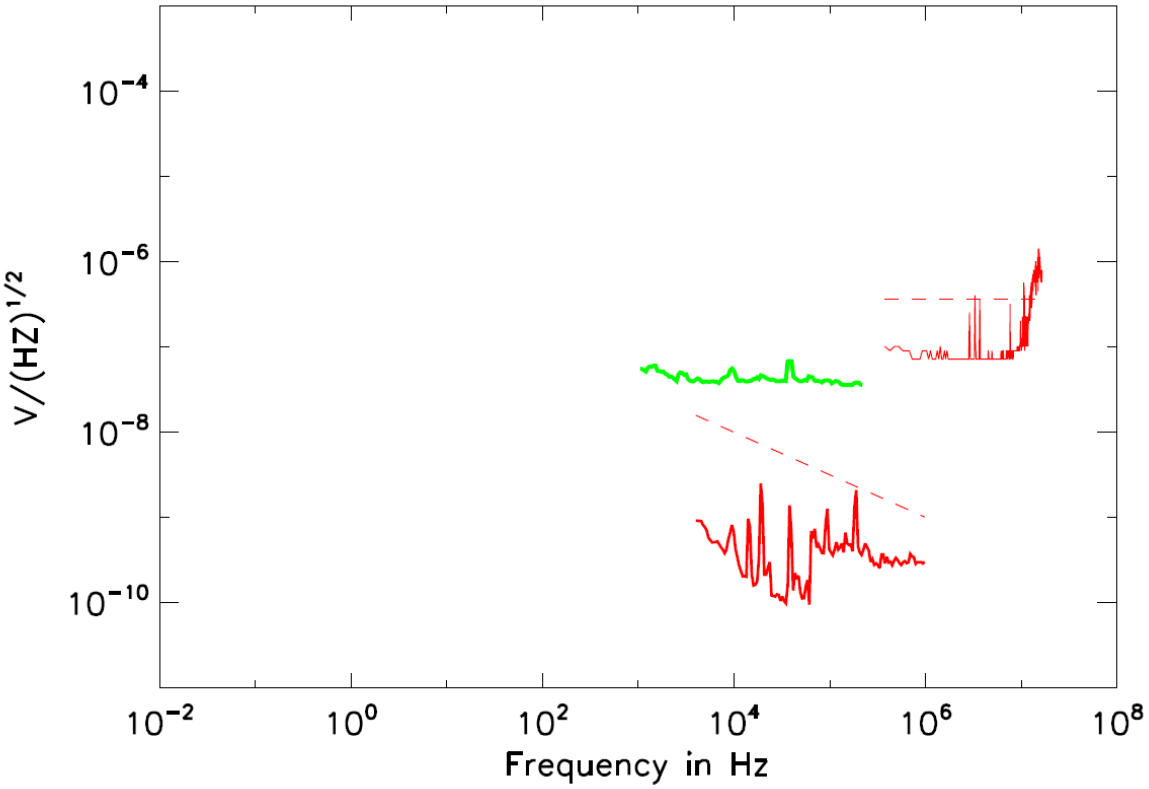

Figure 1 : Red=TNR & HFR, Green = TDS

The Figure 1 displays the RPW MEB electrical sensitivity levels as measured with Flight Model MEB connected to the Flight Models pre-amplifiers. This actually corresponds to the global noise level at the pre-amplifier inputs. The black line curve with diamonds represents the best sensitivity possibly achievable as a function of the frequency (at a given frequency the minimum sensitivity among all the sub-units covering this frequency). The black curve with diamonds/stars represent our reference sensitivity curve. Note that in the case of TNR/HFR, the measurements presented on Figure 1 have been obtained in single mode for TNR and in differential mode for HFR.

2.1 Dynamical ranges

Table 1 summarizes the dynamical ranges for LFR as reported by the LFR team (REF?). This table display also the minimum detectable continuous waveform with this receiver. Table 2 provide the final LFR dynamics including those of the BIAS sub-units. Note that the final DC/LF dynamic is set by the LFR since the BIAS does not have intrinsic saturations. Finally, Table 3 summarizes the dynamical ranges measured by the TNR-HFR team.

LFR configurations	LSB (V)	Minimum detectable Continuous Waveform (mV) =	Measured Dynamics (dB)
V1_DC	9.16E-05	17.1	72
V1_HF	9.16E-05	0.208	73
V12_DC	9.16E-05	1.01	76
V12_AC (Gain 5)	9.16E-05	0.183	77
V12_AC (gain 100)	9.16E-05	0.156	51
B-LF3 (gain 10 on Helmoltz coil)	9.16E-05	2.2	67

Table 1

LFR minimum dynamics	51 dB
BIAS maximum gain (except for F3)	40 dB
Bias maximum attenuation	-24 dB
LF final dynamic range	115 dB

Table 2

TNR-HFR configurations	TNR V1				TNR V1-V2				TNR BMF	HFR V1-V2
Frequency Band	A	B	C	D	A	B	C	D		
Measured Dynamics (dB)	121	118	113	107	118	115	110	104	TBD	108

Table 3

3 SCM PERFORMANCES

The SCM performances are summarized on Figure 2.

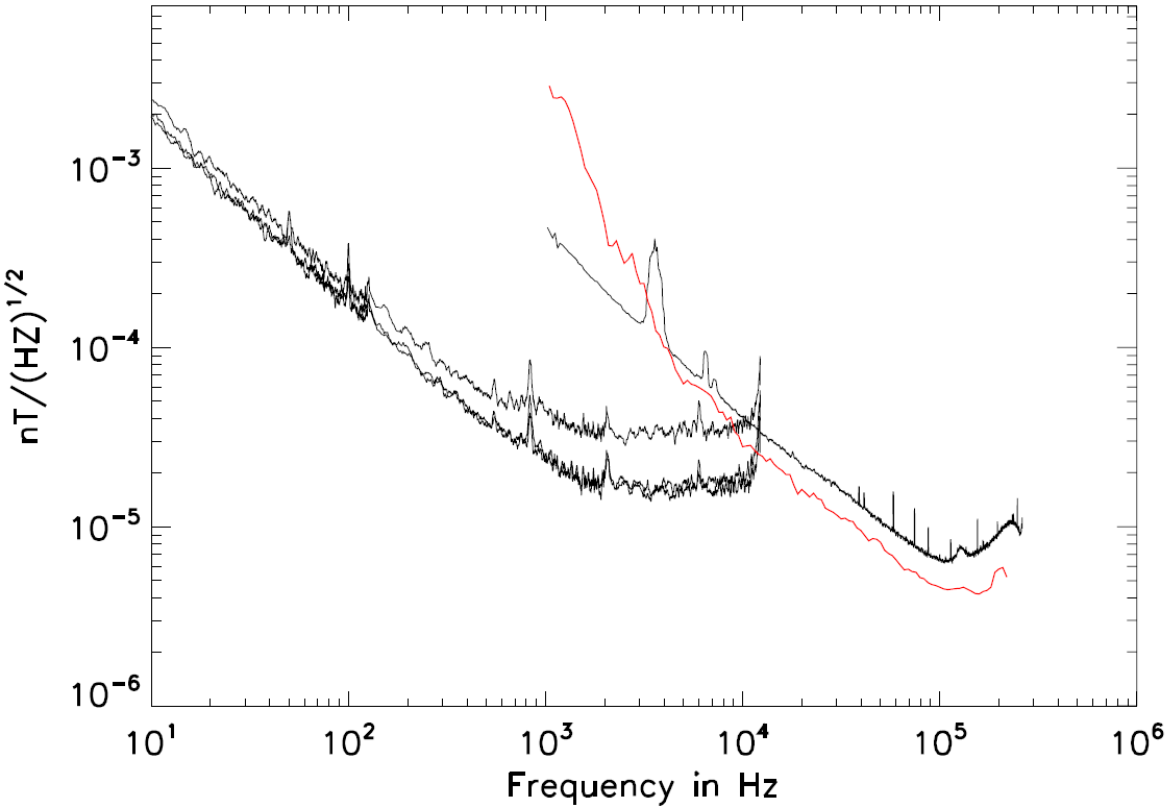

Figure 2

On this Figure the RPW FM SCM sensitivity levels have been measured in TBD conditions.

4 ELECTRICAL ANTENNAS PERFORMANCES

The RPW Electric antennas have been developed and built by the Stellar Scientific company (Berkeley CA, USA), under the supervision of CNES.
Figure 3 represent the final configuration of the RPW antennas, once deployed, with the antenna physical dimensions and tip-to-tip and base-to-base lengths.

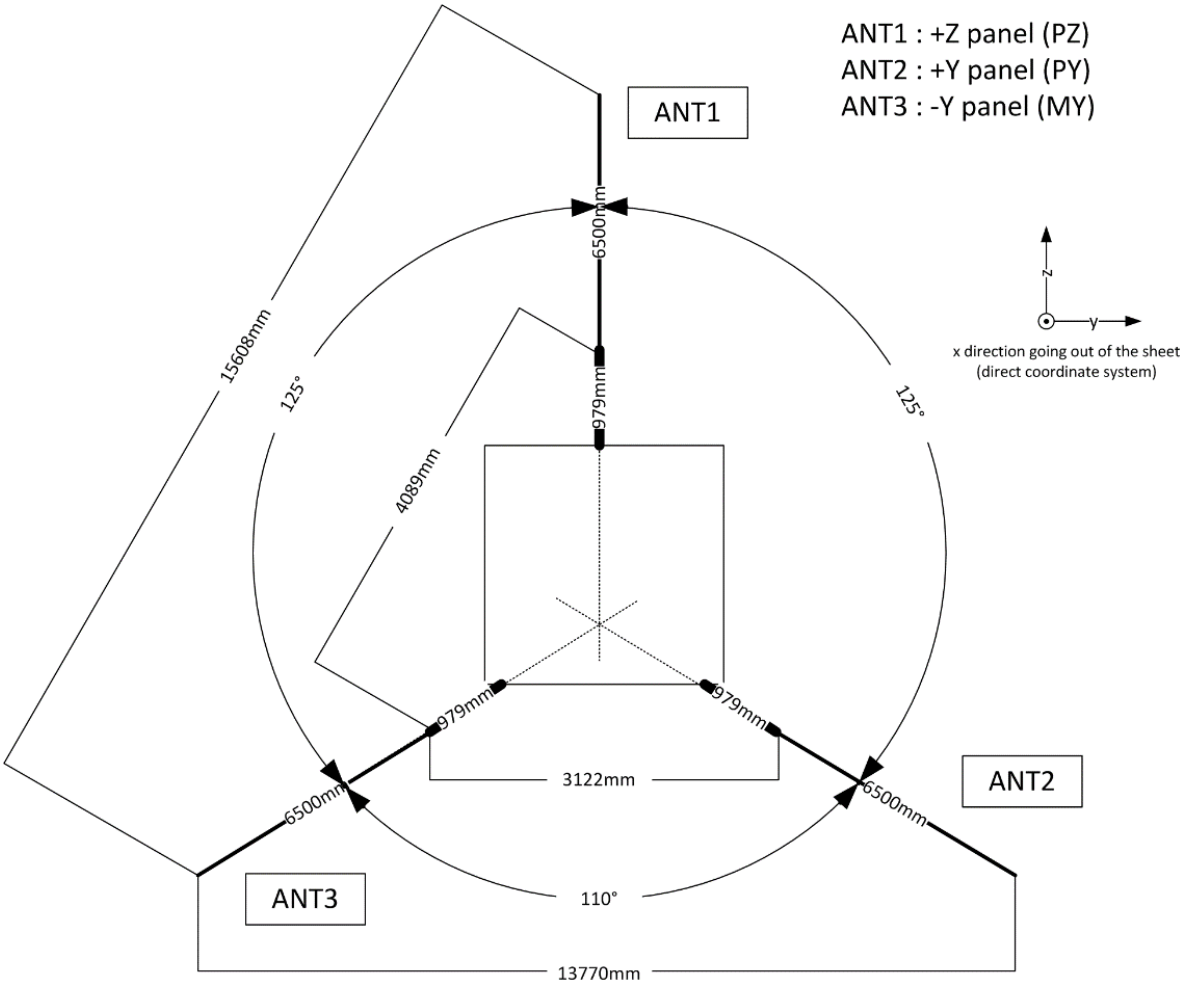

Figure 3

Table 5 provides de naming convention for the three antennas

Serial #	Antenna	Panel	Measurement
FM01	ANT 1	PZ	V1
FM02	ANT 2	PY	V2
FM03	ANT 3	MY	V3

Table 5

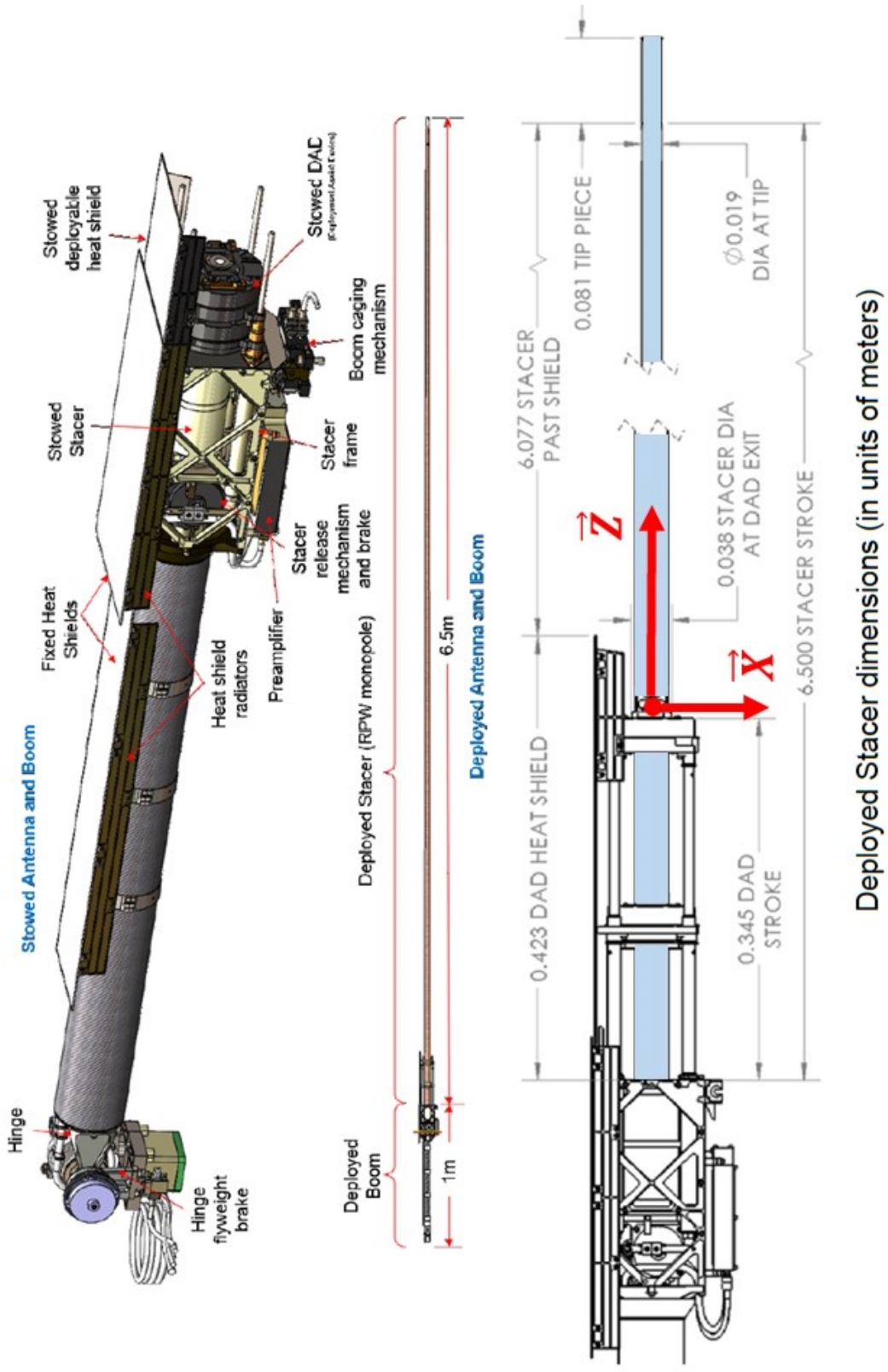

Figure 4 : Antenna design and deployed dimensions

4.1 Thermo-mechanical bending of the Antennas

The design and dimensions of the deployed RPW antennas is provided on Figure 4. Once deployed, the stacer is exposed to Sun and therefore heats up on one side (the non-exposed side seeing dark space). This one side heating will create dilatation on one side and thus a mechanical bending which has been analyzed in [RD10]. The closer to the Sun the more important will be the heating and therefore the bending. Figure 5 (a) displays the modelling of this bending as a function of the heliocentric distance. The diamonds correspond to the data from [RD10]. The thick lines correspond to a best model fit in the form

$$Z = A(R)\sqrt{X} \qquad (1)$$

where X and Z are the coordinates, expressed in meters, of the antenna in a frame represented on Figure 4, with the origin corresponding to the tip of the DAD stroke. A is a parameter which is a function of the radial distance R. Note that the total length of the antennas, i.e. the length colored in blue on the Figure 4 is 6.5 m. The length which is subject to thermal bending is therefore equal to $6.5 - 0.35 = 6.15\ m$. A linear fit of the variation of $A(R)$ provides the following model which can be easily implemented for the analysis of the RPW data.

$$A(R) = 10.5 \times R + 2.0 \qquad (2)$$

where R is in Astronomical Units and A is in $(\mathrm{m})^{1/2}$. This model is represented by the dotted line on Figure 5(b).

The thermoelectric bending described here will have impacts both on the antennas effective lengths and vectors at radio frequency and possibly for the DC electric field measurements.

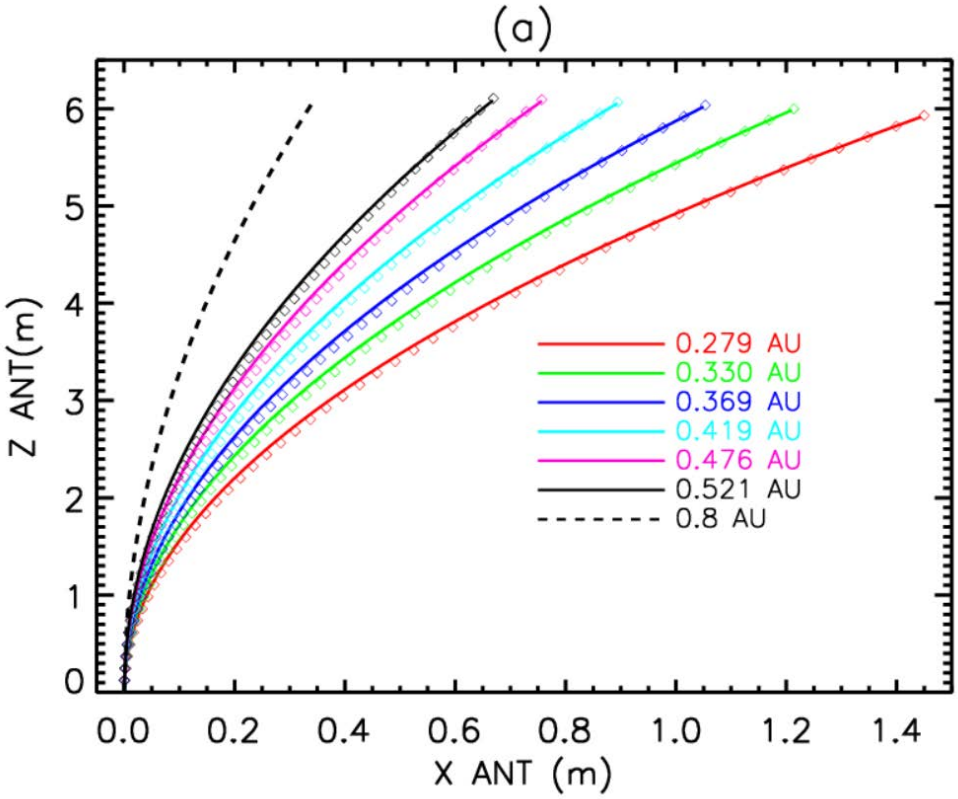

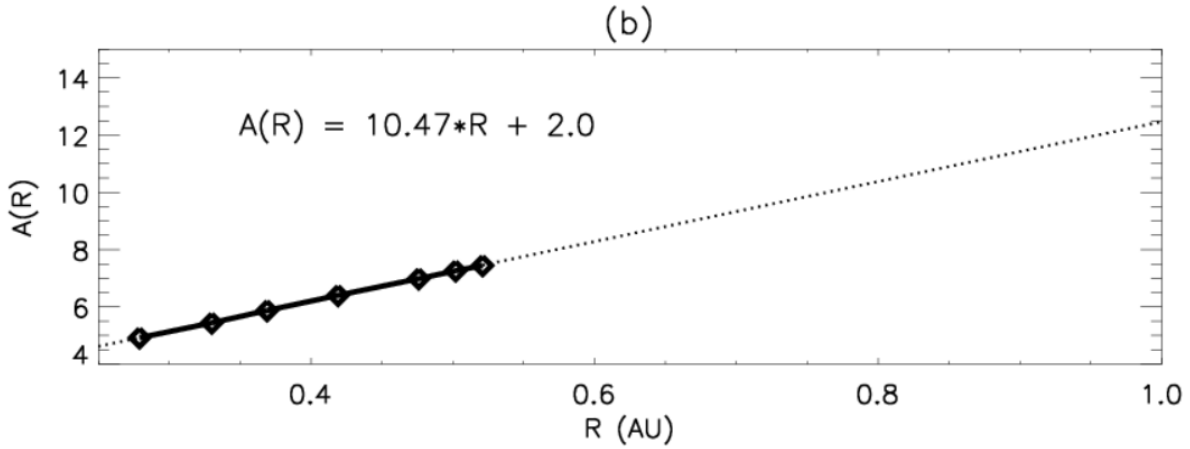

Figure 5: Antenna thermomechanical bending parameter A

4.2 Antennas in the DC/LF domain

RPW will measure in space electric potential difference between antennas and not electric DC/LF fields directly. The latter will be obtained by dividing the measured potential differences by effective antennas lengths L_{eff}^{DC}. It is extremely difficult, if not currently impossible, to define L_{eff}^{DC} on ground. Measurements are not possible since it is currently impossible to reproduce the solar wind plasma conditions on ground, in a plasma chamber for instance. What is possible to do is to use appropriate tools such as SPIS[1] (Spacecraft Plasma Interaction Software) developed by ESA, CNES & ONERA to try to obtain a more or less reasonable estimate of L_{eff}^{DC}. Note also that the DC effective lengths will finally be determined in space by using data from other instruments[2]. In first order, and it has been done in the previous issue of this document, it is possible to assume that the DC/LF antenna effective length in differential mode (difference of potential between two antennas) is comprised between

- $L_{eff\ min}^{DC} = 3.122$ m, which is the minimum base-to-base length (actually the ANT2-ANT3 base-to-base length
- and $L_{eff\ max}^{DC} = 15.608$ m, which is the maximum tip-to-tip length (actually the ANT1-ANT3 tip-to-tip length).

In the next subsection, we will compare these estimates with the results of SPIS simulations performed by S. Guillemant in [RD13].

4.2.1 SPIS RPW simulations

The general idea of the simulations performed in [RD13] for RPW is to apply in the simulation box (i) an external magnetic field varying in amplitude and (ii) a protons and electrons plasma drifting at a typical solar wind speed of and to compute the equilibrium electric potential of the three RPW antenna under the influence of both the ambient solar wind plasma and the resulting **VXB** electric field. All the details of these simulation for RPW can be found in [RD13]. Table 5 below summarizes the main results.

[1] http://dev.spis.org/projects/spine/home/spis
[2] The measured DC electric field will be compared to the VXB field obtained from the Magnetometer data (B field) and the Solar Wind Analyzer data (for the solar wind bulk speed V).

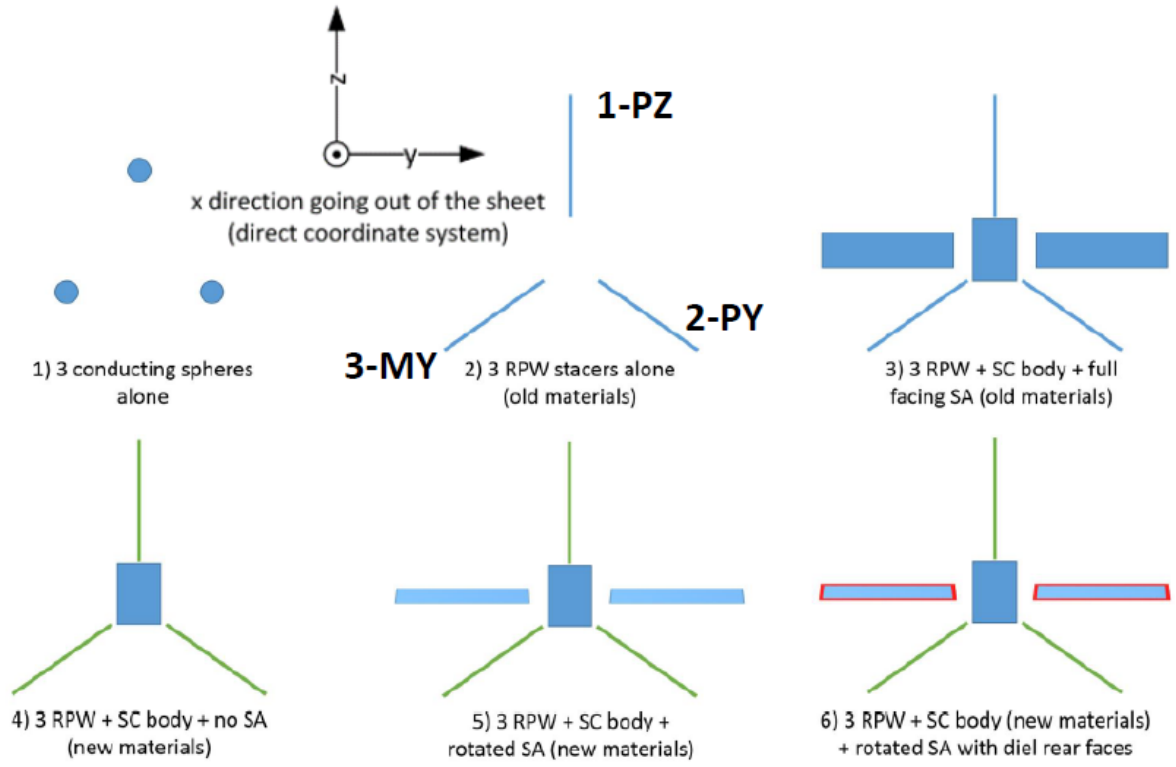

Configuration	1	2	3	4	5	6
ΦRPW1 (V)	13.15	Range	Range	5.04	3.58	1.69
ΦRPW2 (V)	15.93	Range	Range	7.53	6.37	1.82
ΦRPW3 (V)	22.35	Range	Range	8.81	6.69	4.01
Leff 1-2 (m)	**6.80**	**5.83**	**4.83**	**6.28**	**7.05**	**0.33**
Leff 1-3 (m)	**6.80**	**5.83**	**4.83**	**9.51**	**7.86**	**5.88**
Leff 2-3 (m)	**6.40**	**0.00**	**0.00**	***3.23***	**0.82**	**5.55**
Lgeo_min 1-2 (m)	7.59	4.12	4.12	4.12	4.12	4.12
Lgeo_max 1-2 (m)	7.59	15.65	15.65	15.65	15.65	15.65
Lgeo_min 2-3 (m)	7.01	3.50	3.50	3.50	3.50	3.50
Lgeo_max 2-3 (m)	7.01	14.15	14.15	14.15	14.15	14.15

Table 5 : Summary of the SPIS simulations for RPW

On the Figure above the Table, are shown various antenna configurations for which SPIS simulations have been performed. The configurations go from the simplest one, with three sphere antennas alone in the Solar Wind, to the most comprehensive one, with actual antenna geometry, plus S/C body and solar panels. Configuration 5 is the one closest to real case in space.

L_{eff}^{DC} is typically between 7 and 8 m for the ANT1-2 or ANT1-3 dipoles (along the Z axis). The L_{eff}^{DC} for ANT2-3 is clearly not well simulated since in for this dipole the resulting ***VXB*** was not in a favorable orientation. What still need to be done is the global simulation described on Figure 6.

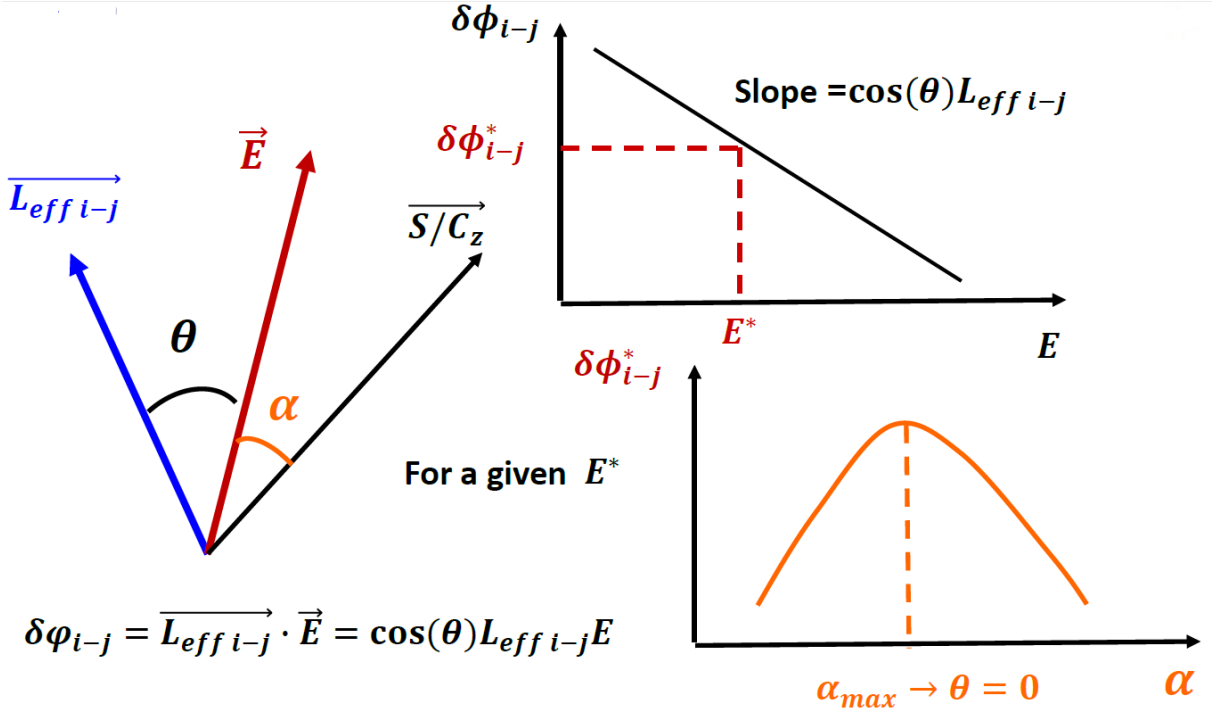

Figure 6

For an ambient electric field $\vec{E}$ and an actual effective length $\overrightarrow{L_{eff\,i-j}}$ in the simulation box as displayed on the left hand side of Figure 6, the potential difference $\delta\varphi_{i-j}$ measured in the actual $i-j$ direction will be $\delta\varphi_{i-j} = \overrightarrow{L_{eff\,i-j}} \cdot \vec{E} = \cos(\theta)L_{eff\,i-j}E$. Since the actual $i-j$ direction is not known, it is possible to retrieve it by performing several simulations where the angle α between the imposed $\vec{E}$ direction and, for instance, the known $\overrightarrow{S/C_Z}$ direction would change. Then for a given amplitude E^* of the imposed electric field, the α_{max} value corresponding to the maximum $\delta\phi^*_{i-j}$ will correspond to $\theta = 0$ and therefore to the determination of the actual orientation of the $\overrightarrow{L_{eff\,i-j}}$ direction in the spacecraft frame (given by α_{max}).

These simulations with a varying $\vec{E}$ orientation have still not been performed. The main reason is that they are very time consuming and not stable. A solution to this problem should be found sometime before the end of the cruise phase of the mission, in order to be ready for interpreting the RPW DC/LF data.

For the time being and the purpose of this document we will assume

- $L^{DC}_{eff\ min} = 3.122$ m, which is the minimum base-to-base length (actually the ANT2-ANT3 base-to-base length
- and $L^{DC}_{eff\ max} = 8$ m, which is the maximum of the effective length reported in Table 5 (ANT1-ANT3 direction) plus some margin.

4.2.2 Spacecraft Electrostatic Cleanliness

Several Requests for Deviations have been raised by either spacecraft or payload subsystems. Assessment have been performed by ESA and the Prime which lead to an overall acceptable level of electrostatic perturbations for the RPW measurements. Among those

- The PAS paint
- The Soo-HI
- The SPICE.

To be developed

4.3 Antennas in the HF/radio domain

4.3.1 Antennas Gain and effective lengths from simulations

For the RPW antennas in the radio domain, it is necessary to determine the total gain ΓL_{eff}^{HF} of the electric sensors. This gain links the receiver voltage power spectral density V_R^2 in V^2/Hz and the source brightness in $W/m^2/Hz/sr$. For instance in the case where the Quasi Thermal Noise (QTN) and the galaxy radio emission are observed by an antenna with a given gain the relation can be written (see [RD4]):

$$V_R^2 = V_{noise}^2 + \Gamma^2 V_{QTN}^2 + \frac{4\pi}{3} Z_0 \Gamma^2 L_{eff}^2 B_{Gal} \text{ with } Z_0 = \sqrt{\mu_0/\epsilon_0} \sim 120\pi \quad (1)$$

In the expression above V_{noise}^2 is the receiver and pre-amplifier intrinsic noise, B_{Gal} is the Galaxy brightness and Γ is given by $\Gamma = \frac{C_A}{C_A + C_S}$, with C_A and C_S being the antenna and stray capacitances, respectively. The variation of the antenna capacitance as a function of the frequency f is given by:

$$C_A(f) = \frac{\epsilon_0 \pi}{k} \frac{\tan(kL)}{\log\left(\frac{L}{a}\right) - 1} \text{ with } k = \frac{2\pi f}{c} \quad (2)$$

In the above formula we assume that the antenna is a cylinder of physical length L and radius a. The measurements of the stray capacitance C_S are described in more details in [RD1 & RD13] and are summarized in Table 6 at the end of this section.

For the dipole case we use formula (2), replacing L by half the length of the physical dipole (between the tip of the antennas, that is $2L = 15.608$ m), and taking for a the average radius of the conical stacer antennas, $a = 1.5$ cm

The monopole case can be roughly modeled as the one of an antenna on an “infinite ground plane”: we must then take for L the physical length of the antenna, that is $L = 6.5$ m, and multiply the right side of equation (2) by 2.

For small frequencies $f \ll c/2\pi L$ the antenna capacitance is constant as a function of the frequency and equal to $(\epsilon_0 \pi L)/(\log\left(\frac{L}{a}\right) - 1)$. These constant values are summarized in Table 4.

As for the effective length, it is necessary to perform antenna radio simulation. Several such simulations have been performed so far. An initial study [RD5] had been performed on the previous antenna design which was developed by the ACOEM company for CNES. More recently simulations have been performed by two different groups: a first one led by M. Panchenko [RD11] and a second one led by D. Plettemeir [RD12]. These simulations have shown that even though the antennas are physically in the same plane, the spacecraft body has a radio-electric effect of tilting the antennas actual direction in the Sunward direction as displayed on Figure 7. Furthermore, the spacecraft has the effect of shortening the antennas

physical lengths which are given in Table 6. The two simulations provide quite similar parameters.

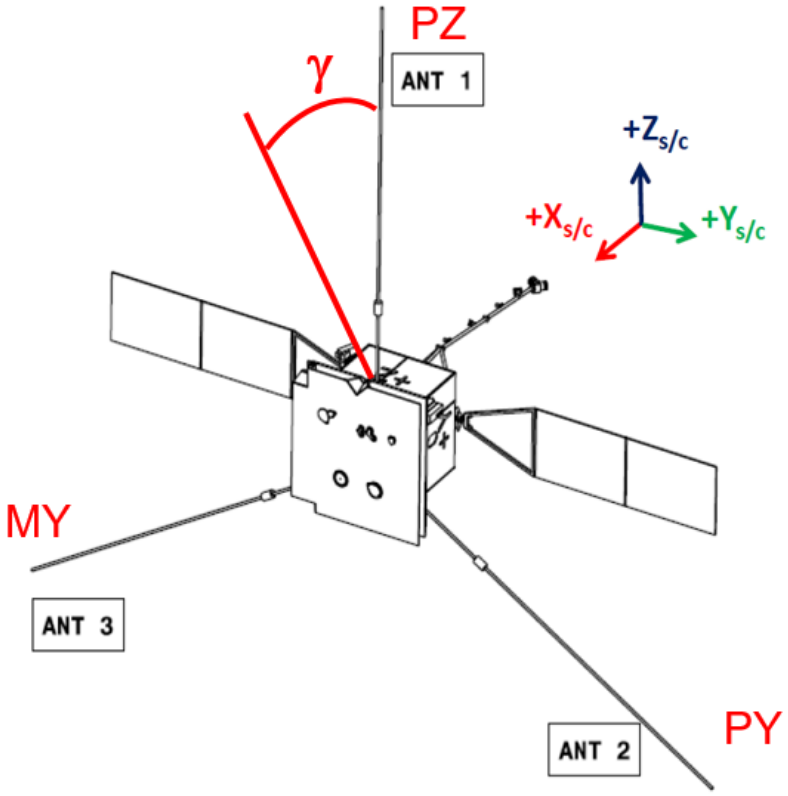

Figure 7

	ANT1 Leff (m)	ANT1 γ (deg)	ANT2 Leff (m)	ANT2 γ (deg)	ANT3 Leff (m)	ANT3 γ (deg)
Plettemeier et al. [RD12]	3.797	8.66	3.385	10.19	3.277	10.13
Panchenko et al. [RD11]	4.41	9.1	3.91	13.6	3.91	13.6

Table 6

In addition Panchenko et al. [RD11] have computed the effective lengths for the dipole cases. The results are given in Table 7 and on Figure 8.

ANT	Mechanical antennas			Effective antenna vectors			
	h, m	θ, deg	φ, deg	h_e, m	θ, deg	φ, deg	γ, deg
PZ	6.5	0.0	0.0	4.41	9.1	-0.4	9.1
PY	6.5	125	90	3.91	132.2	75.2	13.6
MY	6.5	125	-90	3.91	132.3	-75.2	13.6
	Pseudo-dipoles			Effective vectors of dipoles			
Dip. PZ-PY	11.53	152.5	90	7.53	158.1	-90.9	5.6
Dip. PY-MY	10.65	90.0	90	5.60	90.00	90.0	0.0
Dip. MY-PZ	11.53	152.5	-90	7.53	158.2	-89.1	5.6

Table 7: Dipole and monopole effective antennas vectors as obtained from the simulation in [RD11]. The angles θ, ϕ and γ are defined on Figure 8.

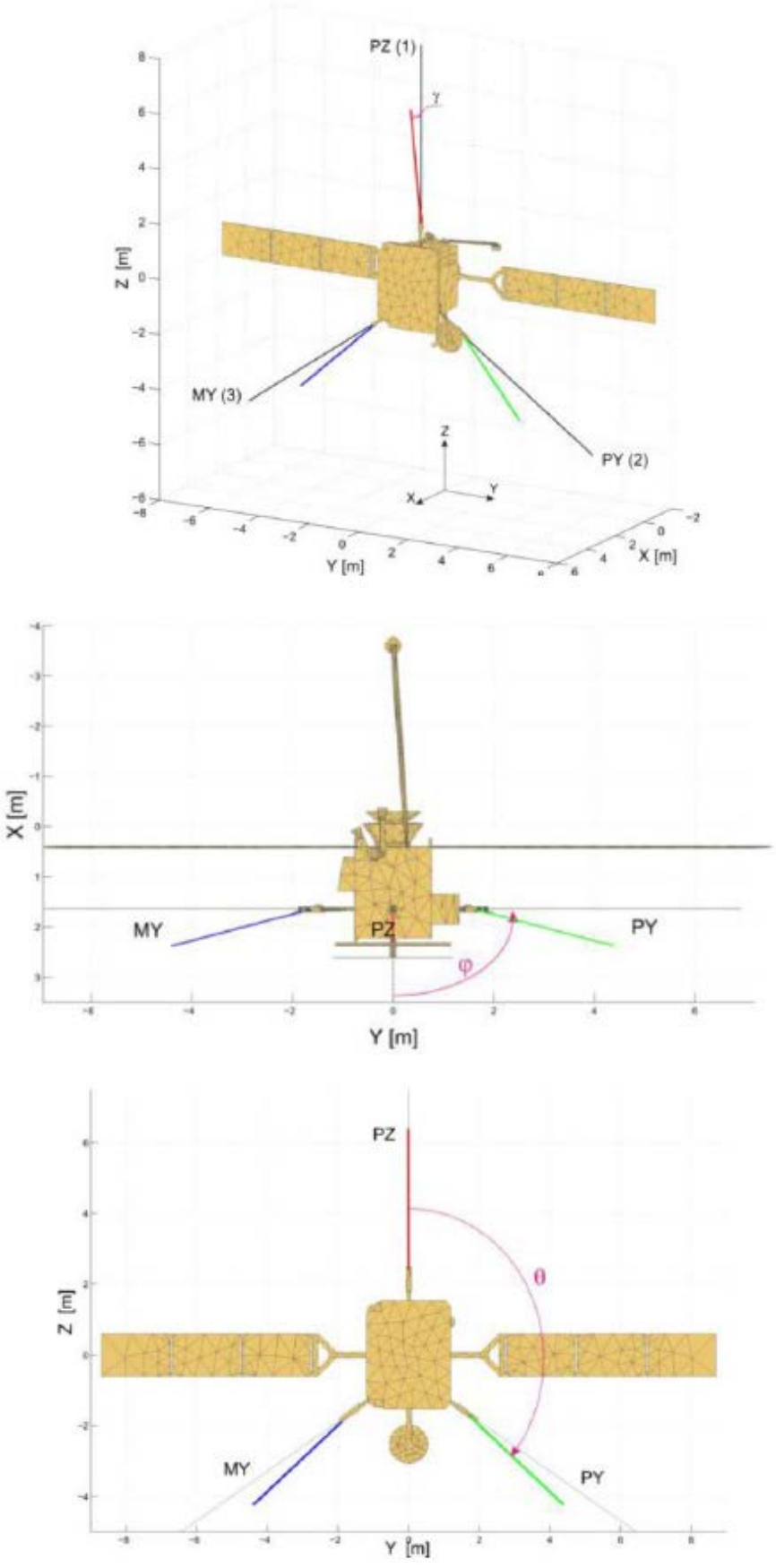

Figure 8

4.3.2 Effect of the thermal bending on the effective antennas vectors

Finally, the effect of the antenna thermal bending described in section 4.1 will also modify the radio-electric influence of the spacecraft body. When all the three antennas are in the same plane, then the effective vectors are tilted towards the Sun by an angle γ given in Table 7. Since the bending is pushing the antennas in the anti-sunward direction, the final effective angle γ will decrease. This decrease is modelled in [RD11] and summarized in Table 8.

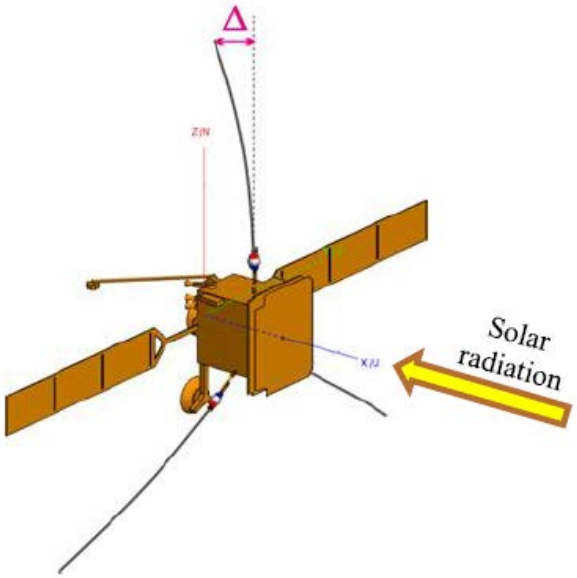

Tip offset	Effective antenna vectors											
	PZ				PY				MY			
Δ, m	h_e, m	θ, deg	φ, deg	γ, deg	h_e, m	θ, deg	φ, deg	γ, deg	h_e, m	θ, deg	φ, deg	γ, deg
0.0	4.41	9.1	-0.4	9.1	3.91	132.3	75.2	13.6	3.91	132.2	-75.2	13.6
0.1	4.41	8.7	-0.4	8.7	3.91	132.3	75.8	13.3	3.91	132.3	-75.8	13.2
0.2	4.41	8.4	-0.4	8.4	3.91	132.4	76.3	13.0	3.91	132.4	-76.2	13.0
0.3	4.41	8.1	-0.5	8.1	3.9	132.5	76.7	12.7	3.9	132.4	-76.7	12.7
0.4	4.4	7.7	-0.5	7.7	3.89	132.6	77.2	12.5	3.89	132.5	-77.2	12.5
0.5	4.4	7.4	-0.5	7.4	3.88	132.7	77.7	12.2	3.89	132.6	-77.7	12.2
0.6	4.39	7.0	-0.5	7.0	3.87	132.7	78.2	12.0	3.88	132.7	-78.2	11.9
0.7	4.38	6.7	-0.5	6.7	3.86	132.8	78.8	11.7	3.87	132.7	-78.7	11.7
0.8	4.38	6.4	-0.6	6.4	3.86	132.9	79.3	11.5	3.86	132.8	-79.3	11.4
0.9	4.37	6.0	-0.6	6.0	3.85	133.0	79.8	11.2	3.86	132.9	-79.8	11.2
1.0	4.37	5.7	-0.6	5.7	3.85	133.0	80.3	11.0	3.85	133.0	-80.3	10.9
1.1	4.37	5.3	-0.7	5.3	3.84	133.1	80.9	10.7	3.85	133.0	-80.8	10.7
1.2	4.37	5.0	-0.7	5.0	3.84	133.1	81.4	10.5	3.84	133.1	-81.4	10.5
1.3	4.37	4.6	-0.8	4.6	3.84	133.2	82.0	10.3	3.84	133.1	-81.9	10.2
1.4	4.37	4.2	-0.9	4.2	3.83	133.2	82.5	10.1	3.84	133.2	-82.5	10.0
1.5	4.37	3.9	-0.9	3.9	3.83	133.3	83.1	9.9	3.83	133.2	-83.1	9.8

Table 8 : The effective antenna vectors for different values of the thermal bending Δ (see figure above the Table)

4.3.3 Free Field measurements and rheometry

- Describe the results made in Figarol or make a reference to an already existing document

- Describe the results of the rheometry measurements made by Pancheko et al. [RD11].

4.3.4 Summary

The Table 6 summarizes the antenna properties in the radio domain. The values for the antenna and stray capacitances have been discussed previously. The values of the effectives antennas lengths are those obtained by simulation (section 4.3.1). For the values reported there, in the monopole case, the min and max values are the values for the PY antennas with a bending Δ=1.5 m and the PX antenna with a bending Δ=0.2 m, respectively. For the dipole case, the maximum Leff is the one for PZ-PY (or MY-PZ, which is the same) while the minimum value is the

		Monopole	Dipole
Antenna capacitance C_A	Physical length *L (m)*	6.5	7.804
	radius *a (m)*	0.015	0.015
	C_A (pF) for f << c/2πL	**71.30**	**41.31**
Cstray (pF)	antenna Cstray FM01 FM02 FM03 FS mean	 76.3 ± 4.0 78.9 ± 3.0 76.2 ± 2.7 74.5 ± 2.0 **76.5 ± 2.9**	
	preamplifier Cstray	33.0	
	Stud Cstray	0.0	
	Cstray	**109.5**	**54.7**
$\Gamma = C_A / (C_A + C_S)$	**Γ for f << c/2πL**	**0.48**	**0.43**
Leff	min	3.83	5.48
	max	4.41	7.53
ΓLeff for f << c/2πL	min	**1.83**	**2.35**
	max	**2.12**	**3.24**

Table 6 : Antenna radio-electrical properties

The Figure 9 displays the variation of the absolute value of ΓL_{eff}^{HF} as a function of the frequency for the ANT monopole case in black and the dipole one in red. The solid and dashed lines represent the curves for the minimum and maximum values of L_{eff}^{HF} respectively. The first peaks at $f^* \approx$ 11.85 MHz (dipole) and $f^* \approx$ 13.9 MHz (monopole) correspond to the "first resonances" implied by $C_A(f^*) + C_S = 0$ and thus $\Gamma \to \pm\infty$. The minimum at $f^{**} \approx$ 19.25 MHz in the dipole case corresponds to $C_A^{\text{Dipole}}(f^{**}) = 0$ and thus $\Gamma = 0$. Note that on RPW, since the maximum frequency of the TNR-HFR is 16 MHz, this minimum at f^{**} will probably be not seen.

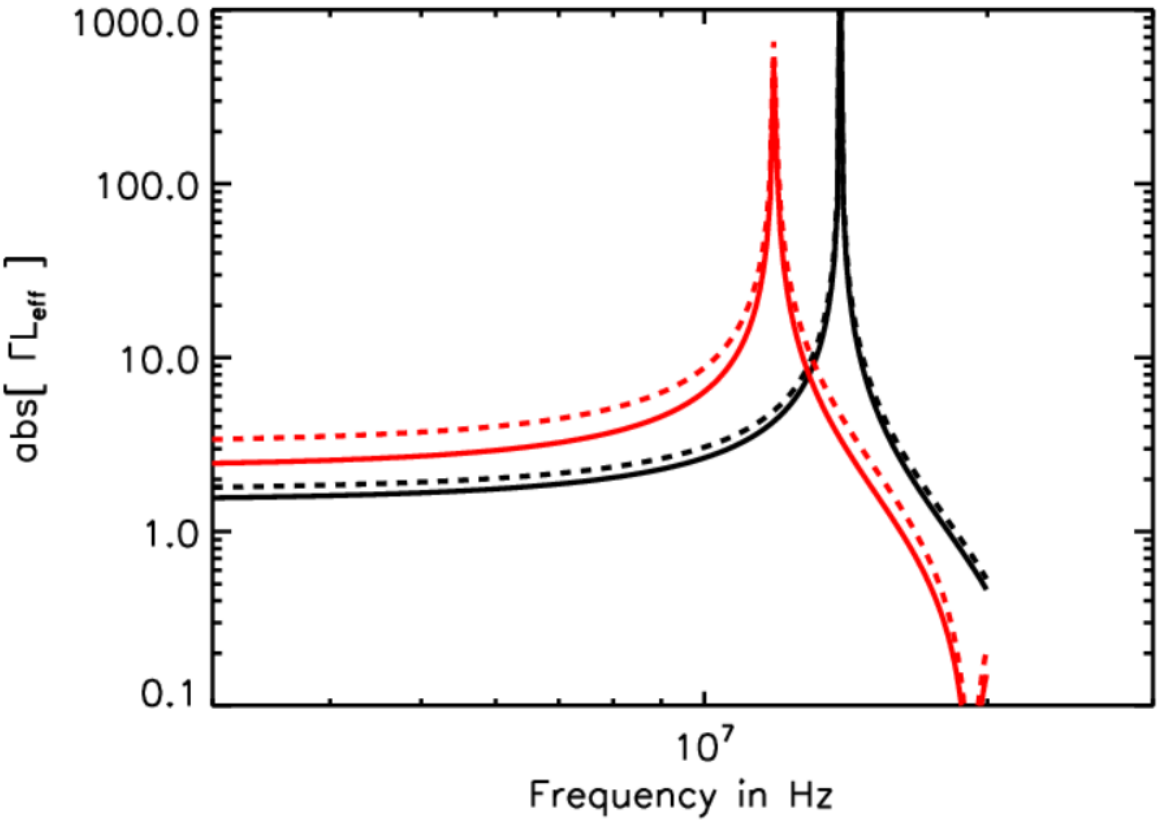

Figure 9

4.4 Radio Direction Finding performances

In principle, because of the antenna configuration for RPW with all 3 antennas being in the same plane, the Direction Finding technique for the localization of solar radio bursts should not be possible. Simulations however have shown, as described in the previous section, that the effective antenna vectors will be tilted towards the Sun because of the radio-electrical effects of the spacecraft body. Complete Direction Finding simulations [RD2 & RD3] have shown that this tilting will be basically enough to fulfill the RPW science requirements with respect to this topic.

Figure 10 display the main results of the [RD2 & RD3] simulations. On this Figure are displayed the uncertainties $\Delta\mathbf{k}$ on the vector of arrival of a Solar radio burst **k**, as a function of the radio-electric tilt angle 90-γ (γ being defined on Figure Panchenko). These uncertainties $\Delta\mathbf{k}$ are displayed for three different errors on the estimate of the antenna effective direction in deg and effective length in %.

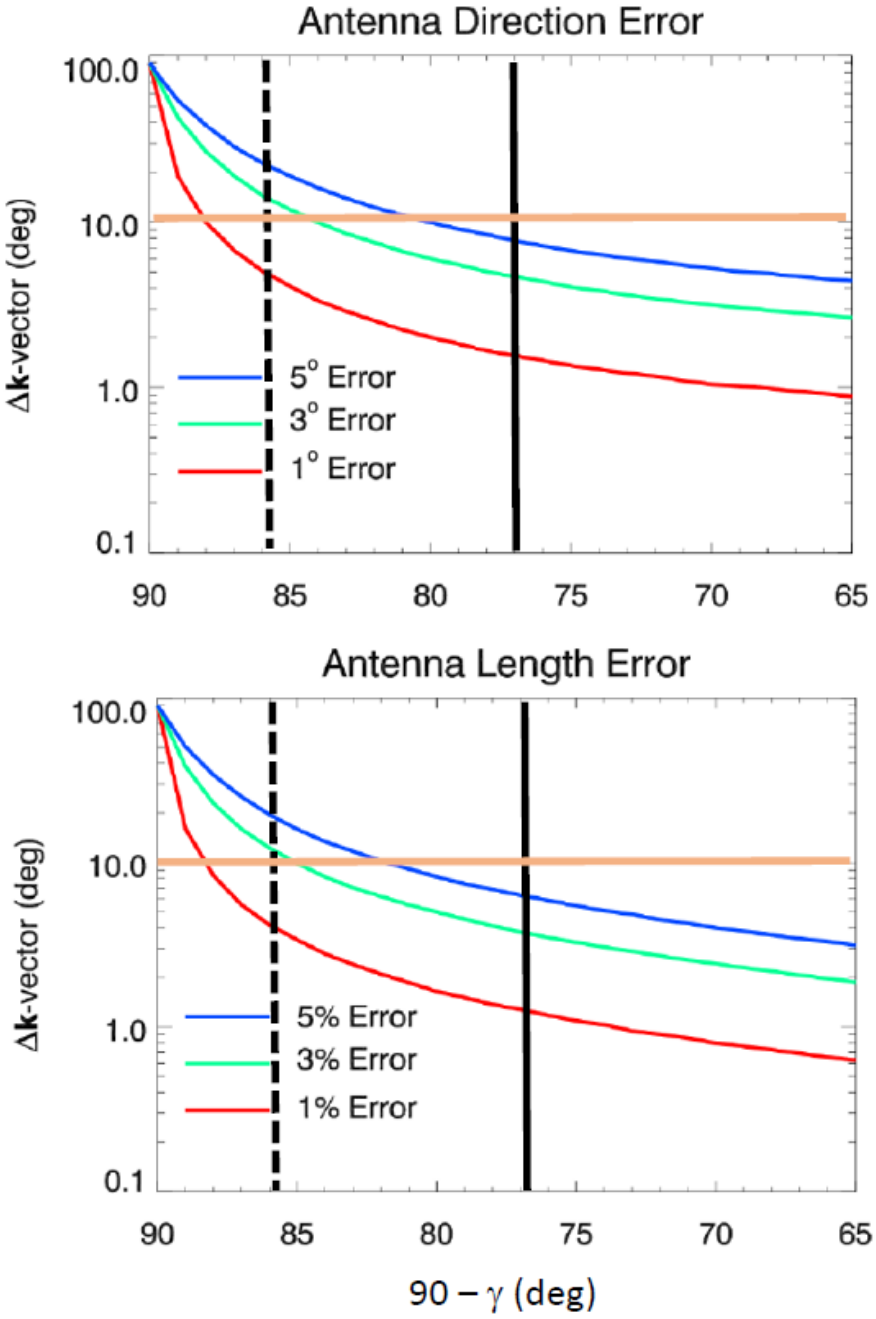

Figure 10 : See text for the detailed explanations

An error of Δk =10° (horizontal orange lines) is acceptable from the science point of view. The vertical dashed and full black lines correspond to the worst case (PZ antenna with Δ=1.45 m at 0.28 AU) and the more favorable case (PY or MY antenna with Δ=0.24 m at 1 AU) for the thermal bending. As one can see the Direction Finding requirement (Δk≤10°) can be obtained with uncertainties on the determinations of the effective antenna lengths and direction less than 5 to 3 % and 5 to 3 ° respectively. Such uncertainties are reachable from both the radio simulations, ground measurements and space calibrations of the antennas once in flight using the observations of the Terrestrial Auroral Kilometric radiations while rolling the spacecraft (see requirement in [RD6]).

5 ELECTRO-MAGNETIC CLEANLINESS

5.1 RPW auto-compatibility

To be written or making a reference to an already existing document

5.2 Electro-Magnetic Cleanliness at spacecraft

Waiting for final evaluation by ESA

6 RPW SYSTEM LEVEL PERFORMANCES AND COMPLIANCE WITH RESPECT TO THE SCIENCE REQUIREMENTS

6.1 System Level Performances

In this section we compare the RPW EM2 performances with the Science requirements described in [AD1].

6.1.1 Natural electric fields in the quasi-DC/LF frequency range

The Figure 11 summarizes the RPW performances for measuring the natural electric fields in the quasi-DC/LF frequency range. This Figure has to be compared to Figure 7 of the science requirements document [AD1].

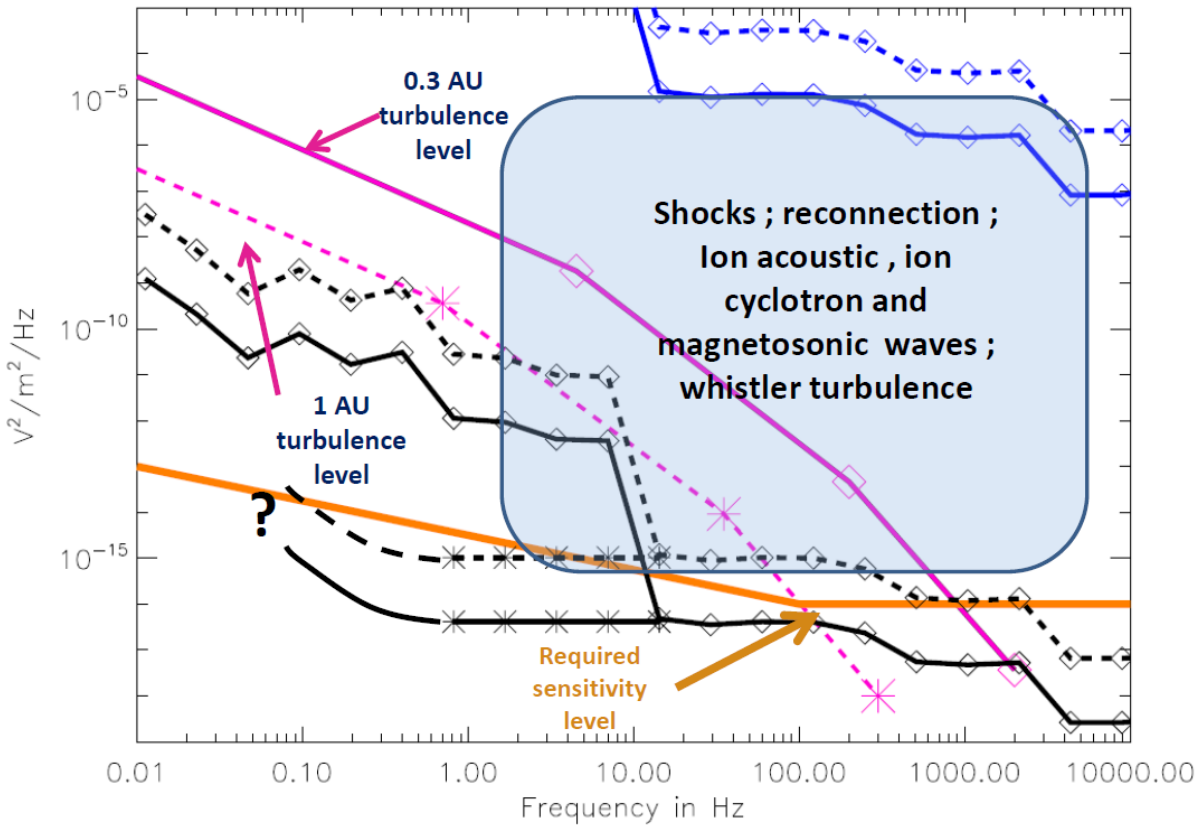

Figure 11

Sensitivities

On Figure 5 the required RPW sensitivity level is displayed by the orange line and the required dynamical ranges are such to allow the measurements of the physical phenomena reported on this Figure. The black solid and dashed lines with diamonds represent the electrical sensitivity levels as reported in section 2.1. The solid & dashed correspond to the minimum & maximum L_{eff}^{DC}.reported in section 4.1.

For frequencies lower than 10-20 Hz, it is not possible to conclude whether the required sensitivity can be achieved by running the LFR waveforms capture in the frequency mode F2, with the BIAS gain 5 and during 10 minutes (solid & dashed black curves with stars). This will depend on the characterization of the 5 Hz high pass filter which will be performed for the final calibrations.

For frequencies larger than 10 Hz, the required sensitivity can only be achieved if the final minimum L_{eff}^{DC} in differential does not reach the minimum possible value of 3.1 m. This point will be checked for the final version of this report for the Flight Model and is pending the output of the current SPIS simulations.

Dynamical ranges

Concerning the dynamical range, the blue curves on the top part of Figure 11 are obtained by adding the ranges reported in Table 2 to the sensitivity levels. RPW is compliant below ~100 HZ. Above this frequency, RPW may be compliant depending on the final L_{eff}^{DC}, which is pending on SPIS simulations. Note also that different antenna couples, with different effective lengths, could be used to reach the required sensitivities or maximum signal observed, depending on the science objective one wants to study.

6.1.2 Thermal noise, Langmuir waves, Type III bursts and galactic background in the radio domain

Sensitivities

The Figure 6 displays simulated QTN curves and the typical Galaxy noise model as they will be seen by the current RPW instrument. The square root of the left hand side of equation (1), expressed in *nV/Hz$^{1/2}$*, is displayed as a function of the frequency in Hz. The thermal noise curves are displayed in red with solid lines. The orange curves correspond to the Galaxy noise observed by a monopole RPW antenna while the magenta curves correspond to the dipole case. The solid and dashed lines represent the curves for the minimum and maximum values of L_{eff}^{HF} respectively. The dotted magenta line represent the Galaxy observed in dipole with an effective length of 7 meters.

The solid blue curve represents on Figure 12 the requirement sensitivity level as defined in last version of [AD1]. The solid black curve with stars represent the sensitivity achieved with the EM2 MEB, as described in section 2.1. These measurements have been obtained in single mode for TNR and in differential mode for HFR.

As can be seen, the achieved noise is above the requirement. The HFR (above 1 MHz) measured sensitivity level is only compliant if the final L_{eff}^{HF} is sufficiently high. In dipole (magenta curves on Figure 6), the Galaxy can be seen only if $L_{eff}^{HFdipole}$ is larger than 6 meters (magenta dotted curve) or ΓL_{eff}^{HF} at low frequencies larger than 3.

We recall here that measuring the galaxy noise with RPW is crucial in order to determine the final receiver noise in this frequency range (see the technique described and used in [RD4]) and to confirm the ground simulations of ΓL_{eff}^{HF}.

For TNR (below 1 MHz), although not compliant, the sensitivity level allows still to observe the thermal noise in the worst case (lowest left QTN curve in red on Figure 12.

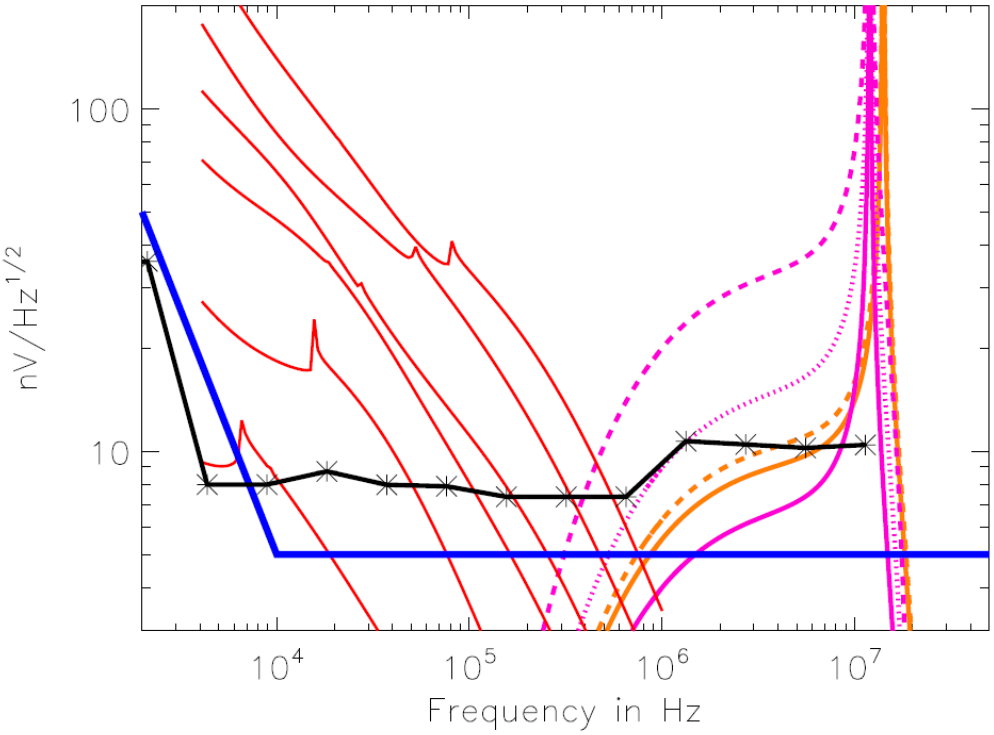

Figure 12

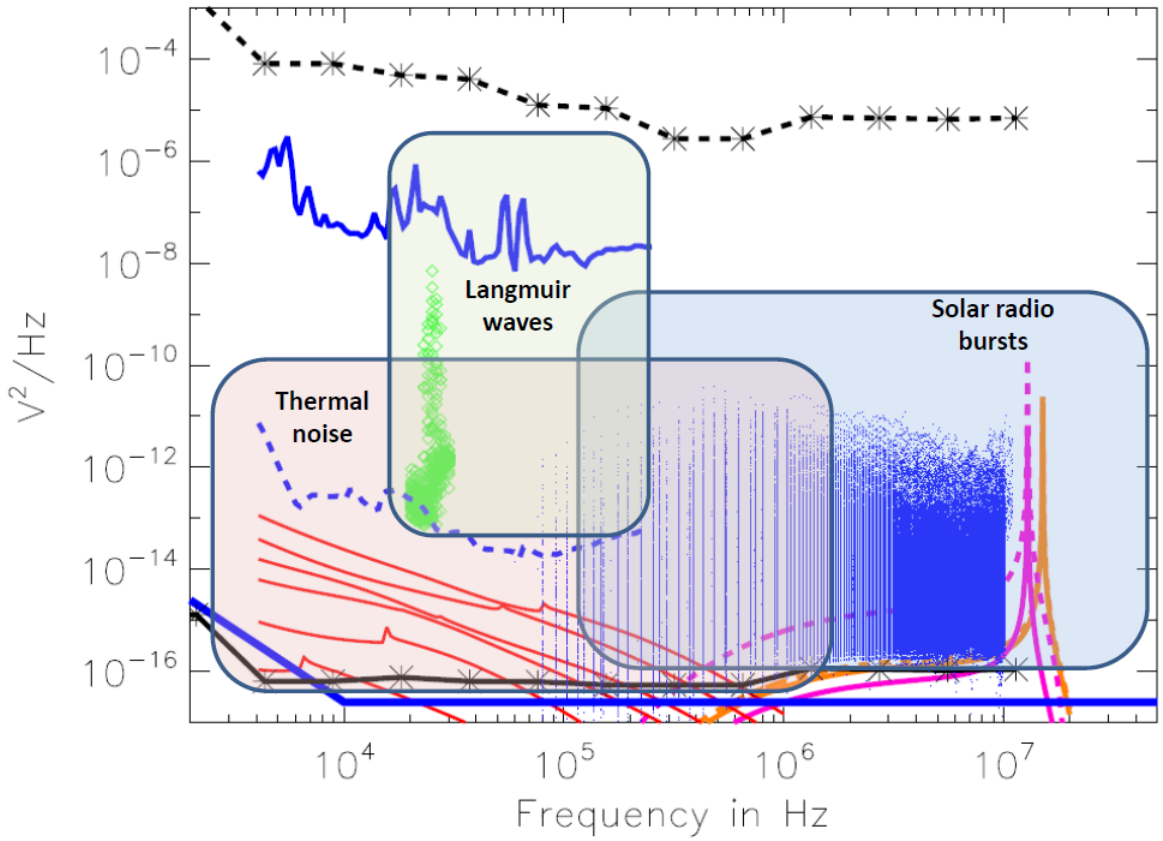

Figure 13

Dynamical ranges

The Figure 7 displays the QTN curves and the typical Galaxy noise as on Figure 6 but in V^2/Hz this time. In addition we have overplot the Langmuir waves and solar Type III radio levels as measured by the WIND spacecraft and used to set the requirement on Figure 7 of [AD1].

The TNR-HFR noise level to which the dynamical range reported in Table 3 has been added is represented by the black dashed curve with stars. It can be seen on this Figure that RPW is fully complaint in terms of dynamics in this frequency range.

6.1.3 Performances for measuring the magnetic field fluctuations

The Figure 8 displays the various natural magnetic field fluctuations which will be observed by RPW and which have been used in order to set the requirement defined by Figure 10 in [AD1]. On this Figure we have represented the sensitivity level reported in section 3 by the blue full line with diamonds and the sensitivity level plus the dynamic range in blue dashed lien with stars.

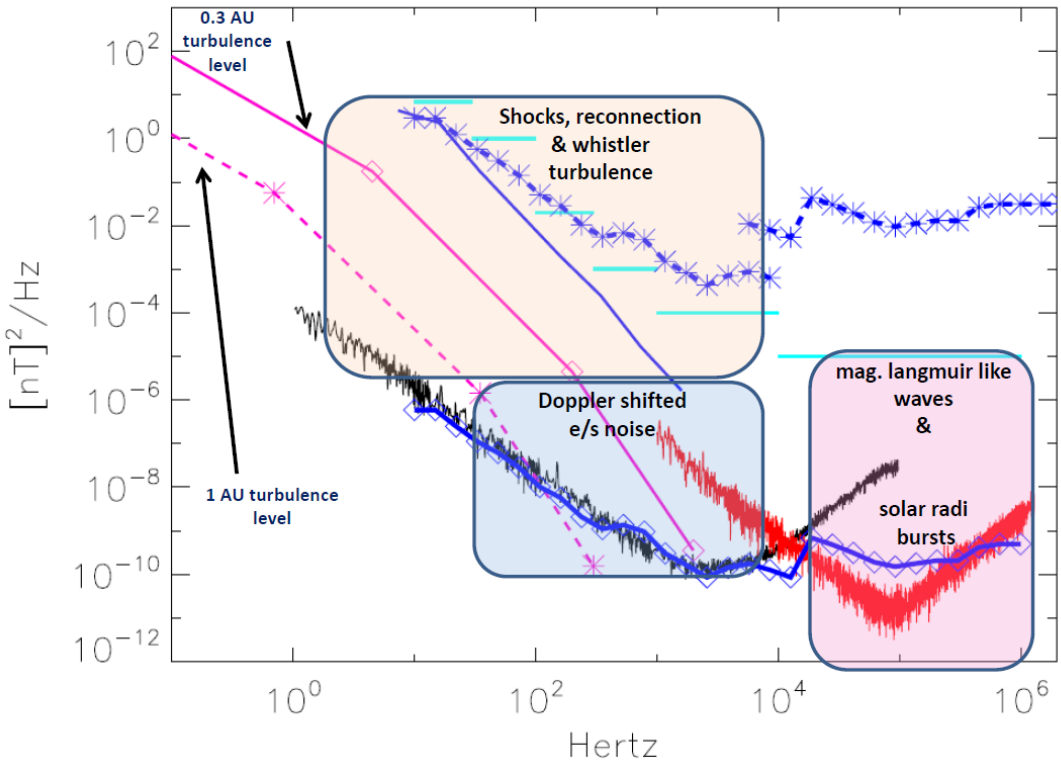

Figure 8

As can be seen on Figure 8, RPW is compliant with respect to the dynamical range. With respect to the sensitivity requirement is compliant in the LF domain up to roughly 10 kHz but is not currently compliant above 10 kHZ. This non-compliance is actually artificial since the TNR sensitivity is actually below the SCM one. One has thus to wait for the final calibration before the FM delivery before being able to assess the actual and final SCM sensitivity for all frequencies

6.2 Performance versus Requirements Compliance Matrix

In this section we demonstrate the RPW compliance to the Science requirements described in [AD1].

Requirement Number	Requirement Description	Status & Justification
REQ-RPW-SCI-0001	The global spacecraft (bus + solar panels + high gain antenna) electric potential variations along the orbit have to be modeled. Particularly should be investigated the potential dependence on (i) the solar wind electron properties (ii) the spacecraft surface electrical properties (conductivity, photoelectron and secondary electrons *etc* …). (iii) the solar UV intensity	**Open** **Ongoing SPIS simulations and discussions within the EMC Working Group**
REQ-RPW-SCI-0002	RPW shall measure spacecraft potential and its variations along the orbit. RPW shall be able to measure the satellite potential	**Open** **RPW can measure V1_DC with a 17 mV accuracy. For a typical S/C**

	variations at least up to 1kSs with relative error better than 10%.	**potential of 5 V this provide a relative error better than 1 %** **However, ongoing SPIS activities in order to estimate the platform electrostatic effects on the S/C potential measurements by RPW**
REQ-RPW-SCI-0003	To address science objectives on solar wind turbulence, shocks, reconnection and current sheets, RPW shall characterize the electric fields in the quasi-DC to 10 kHz frequency range. RPW shall provide both waveform and spectral data in this frequency range.	**Compliant** **See instrument description in [RD6]**
REQ-RPW-SCI-0004	To address shock, reconnection and current sheet objectives, in the quasi-DC-10kHz range (waveform data), RPW shall be able to measure electric fields with amplitudes up to at least 500mV/m and at least 0.1 mV/m resolution. To address turbulence objectives RPW shall be able to measure, in the same frequency range, electric fields with sensitivity at least 0.01 mV/m.	**Compliant for the 500 mV/m with V_{12_DC}=1 mV (see table 1) and, 77 dB of dynamic range and Leff=3.1 m on gets a max amplitude of 2000 mV/m** **Pending on SPIS simulations for the sensitivity with V12_AC(gain 1000) = 0.15 mV and Leff=10 m one gets 0.01 mV/m of sensitivity**
REQ-RPW-SCI-0005	The overall RPW electric sensitivity level of electronics in the quasi-DC to 10 kHz frequency range shall be better than the expected plasma and photoelectron noise levels. For this purpose RPW electronics noise level shall be better than 10^{-16} $V^2/m^2/Hz$ at frequencies above 100 Hz and 1/f increase at frequencies below 100 Hz (see orange curve in Figure 7).	**Compliant below ~100 Hz** **Open above ~100 HZ, depending on the final DC/LF effective length. Pending on SPIS simulations**
REQ-RPW-SCI-0006	The RPW dynamic range in the quasi-DC to 10 kHz frequency range shall allow measuring waves and broad-band signals with power spectral densities up to 10^{-5} $V^2/m^2/Hz$.	**Compliant below ~100 Hz** **Open above ~100 HZ, depending on the final DC/LF effective length. Pending on SPIS simulations**
REQ-RPW-SCI-0007	The global spacecraft (bus + solar panels + high gain antenna) electric potential disturbances at the location of the ANT monopoles shall be minimized. This strongly affects successful addressing of almost all other RPW science requirements dealing with the frequency range quasi-DC to 10kHz. This requirement drives the specific RPW EMC requirements.	**Open** **Pending on the SPIS simulations and ESA EMC Working Group activities**
REQ-RPW-SCI-0008	RPW shall measure and characterize, accordingly to its science objectives, high resolution electric field waveforms enabling observations of Langmuir waves in the inner	**Open** **Pending on TDS characterization and calibrations at system level**

	Heliosphere. The measurement shall cover frequency range from 500 Hz (or less) to 200 kHz and amplitudes from 0.1 mV/m to 300 mV/m.	
REQ-RPW-SCI-0009	RPW shall measure and characterize, accordingly to its science objectives, electric field waveforms with a resolution sufficient for detection of electric field signatures of interplanetary dust impacts. The measurement shall cover frequencies up to 200 kHz and amplitudes from 3 mV/m to 300 mV/m.	**Open** **Pending on TDS characterization and calibrations at system level**
REQ-RPW-SCI-0010	Because of telemetry limitations it will not be possible to transmit all the RPW waveform snapshots concerning **Langmuir waves**. RPW should therefore perform statistical measurements of the corresponding snapshots power distributions.	**Compliant** **See TDS description in TBD document**
REQ-RPW-SCI-0011	Because of telemetry limitations it will not be possible to transmit all the RPW waveform snapshots concerning **dust impacts**. RPW should therefore perform statistical measurements of the corresponding snapshots power distributions.	**Compliant** **See TDS description in TBD document**
REQ-RPW-SCI-0012	RPW shall characterize, accordingly to its science objectives, the electric part of the waves that play a role in the solar wind physics in the 10 kHz to 16 MHz frequency range.	**Compliant** **See instrument description in [RD6]**
REQ-RPW-SCI-0013	Each ANT monopole has to behave at high frequency, in terms of the emission diagram and impedance, like a monopole of a given length *L* and diameter *D.*	**In principle compliant** **But pending on the final antenna simulation and tests in radio domain**
REQ-RPW-SCI-0014	Given the solar wind density and temperature variations reported in section 3.3 and the corresponding Debye Lengths, L has to be larger than 5 meters in order to allow correct Thermal Noise measurements. The upper limit for L shall be compatible with the mechanical requirements from the platform and the RPW overall resources.	**Compliant** **See instrument description in [RD6]**
REQ-RPW-SCI-0015	For minimizing the shot noise perturbations on the thermal noise measurements, the ANT diameter has to be as low as possible, being compatible with the mechanical requirements from the platform and the RPW overall resources.	**Compliant** **See instrument description in [RD6]**

REQ-RPW-SCI-0016	The ANT Preamplifiers have to be mounted on the ANT boom as close as possible to the ANT monopoles in order to minimize the total stray capacitance between them and optimize therefore the antenna gain.	**Compliant** **See instrument description in [RD6]**
REQ-RPW-SCI-0017	The electric sensitivity at the pre-amplifier input shall be lower or equal to 5 *nV/Hz* from 10 kHz to 16 MHz, provided the fact that the final RPW antenna ΠL_{eff} (antenna and stray capacitance gain) in monopole mode is larger than 1.30 (see Figure 8.2) Therefore the overall RPW electric sensitivity level in the 10 kHz – 16 MHz frequency range shall correspond to the orange curve on Figure 8.3 : • 10^{-16} $V^2/m^2/Hz$ at 2 kHz • 10^{-18} $V^2/m^2/Hz$ at 10 kHz and up to 16 MHz	**Pending on final antenna simulations for the ΠL_{eff} for the range above 1MHz** **Not Compliant for the range below 1 MHz but the minimum QTN spectrum can still be somehow observed**
REQ-RPW-SCI-0018	The RPW dynamic range shall allow measuring waves with power spectral densities up to • 10^{-10} $V^2/m^2/Hz$ in the 3 kHz – 300 kHz frequency range • 10^{-12} $V^2/m^2/Hz$ in the 300 kHz – 16 MHz frequency range	**Compliant** **see Figure 7**
REQ-RPW-SCI-0019	The spacecraft bus and payload electromagnetic disturbances at the location of the ANT monopoles & pre-amplifier shall be minimized in order to allow RPW to fulfill the requirement 0017. This requirement is one of the drivers for the specific RPW EMC requirements.	**Pending on the activities of the ESA EMC Working group**
REQ-RPW-SCI-0020	The ANT configuration on the S/C together with mechanical and thermal ANT properties shall allow performing Direction Finding of Type III and Type II radio sources as described in [RD3].	**Pending on the final antenna simulations and measurements in radio domain and on the final antenna configuration on the S/C.** **Note that the preliminary simulation with the initial antenna configuration showed that RPW was compliant.**
REQ-RPW-SCI-0021	Specific S/C calibration rolls shall be performed to calibrate the ANT radio diagram and gain.	**Compliant since in principal taken into account for the Solar Orbiter operations**
REQ-RPW-SCI-0022	RPW shall characterize, accordingly to the science objectives described in [RD1] and	**Compliant** **See instrument description in [RD6]**

	[RD3], the magnetic part of the waves that play a role in the solar wind physics in the ~1 Hz to 1 MHz frequency range.	
REQ-RPW-SCI-0023	The overall RPW magnetic sensitivity level in the 10 Hz – 1 MHz frequency range shall correspond to the sensitivity level of the sensor that has been proposed in [RD3] and studied during phase A. This sensitivity level is represented by the black and red curves on Figure 10.	**In principal compliant (see Figure 8). Need confirmation after the final calibration of the FM**
REQ-RPW-SCI-0024	The RPW dynamic range shall allow measuring magnetic fluctuations with power spectral densities up to • 7 nT^2/Hz for frequencies below 30 Hz • 1 nT^2/Hz in the 30 Hz - 100 Hz frequency range • 2 10^{-2} nT^2/Hz in the 100 Hz – 300 Hz frequency range • 10^{-3} nT^2/Hz in the 300 Hz – 1 kHz frequency range • 10^{-4} nT^2/Hz in the 1 kHz – 10 kHz frequency range • At least 10^{-5} nT^2/Hz in the 10 kHz – 1 MHz frequency range	**compliant (see Figure 8)**
REQ-RPW-SCI-0025	RPW must tolerate, without saturation or impact on performance, field oscillations with spectral densities up to the limits specified in REQ-RPW- SCI-0024. Worst case situation should be considered, where the specified maximum spectral densities are encountered simultaneously in all frequency bands. The signal is assumed to be of the form of broadband oscillations, with peak amplitude Vpeak = 1.41*V_{RMS}.	**TBD with J. Soucek and E. Guilhem**
REQ-RPW-SCI-0026	The spacecraft bus and payload electromagnetic disturbances at the location of the SCM sensor & pre-amplifier shall be minimized in order to allow RPW to fulfill the requirement 0023. This requirement is one of the drivers for the specific RPW EMC requirements.	**Pending on the activities of the ESA EMC Working group**
REQ-RPW-SCI-0027	The SCM sensor orientation on the boom shall be chosen so that it allow RPW to fulfill the requirement 0023.	**Compliant** **See instrument description in [RD6] and TBD with G. Jannet**
REQ-RPW-SCI-0028	RPW shall detect onboard the spacecraft, store and transmit afterwards, all the relevant data associated with interplanetary shock crossings. RPW shall transmit over the course of the mission at least one shock	**Compliant** **See instrument description in [RD6] and [RD6, 7 & 8]**

	crossing every 5 days with a duration up to 13 minutes each.	
REQ-RPW-SCI-0029	RPW shall detect onboard the spacecraft, store and transmit afterwards, all the relevant data associated with in-situ Type III bursts. RPW shall transmit over the course of the mission at 100 of such events with a maximum duration of roughly 120 minutes each.	**Compliant** **See instrument description in [RD6] and [RD6, 7 & 8]**